ISSN 1810-2328, Journal of Engineering Thermophysics, 2017, Vol. 26, No. 2, pp. 256–271. © Pleiades Publishing, Ltd., 2017.

Numerical Study of the Onset of Chemical Reaction and Heat Source on Dissipative MHD Stagnation Point Flow of Casson Nanofluid over a Nonlinear Stretching Sheet with Velocity Slip and Convective Boundary Conditions

S. M. Ibrahim[1], P. V. Kumar[1], G. Lorenzini[2*], E. Lorenzini[3], and F. Mabood[4]

[1]*Department of Mathematics, GITAM University, Visakhapatnam, Andhra Pradesh, 530045 India*

[2]*Department of Engineering and Architecture, University of Parma, Parco Area delle Scienze 181/A, Parma, 43124 Italy*

[3]*Alma Mater Studiorum-University of Bologna, Department of Industrial Engineering, viale Risorgimento 2, Bologna, 40136 Italy*

[4]*Department of Mathematics, University of Peshawar, Pakistan*

Received December 15, 2016

Abstract—The magnetohydrodynamic (MHD) stagnation point flow of Casson nanofluid over a nonlinear stretching sheet in the presence of velocity slip and convective boundary condition is examined. In this analysis, various effects such as velocity ratio, viscous dissipation, heat generation/absorption and chemical reaction are accentuated. Possessions of Brownian motion and thermophoresis are also depicted in this study. A uniform magnetic field as well as suction is taken into account. Suitable similarity transformations are availed to convert the governing nonlinear partial differential equations to a system of nonlinear ordinary differential equations and then series solutions are secured using a homotopy analysis method (HAM). Notable accuracy of the present results has been obtained with the earlier results. Impact of distinct parameters on velocity, temperature, concentration, skin friction coefficient, Nusselt number and Sherwood number is canvassed through graphs and tabular forms.

DOI: 10.1134/S1810232817020096

HIGHLIGHTS

- MHD stagnation point flow of Casson nanofluid is analyzed.
- Flow and heat transfer characteristics are probed in the presence of slip and convective boundary conditions.
- Nonlinear stretching phenomenon is appointed.
- Skin friction coefficient, Nusselt number and Sherwood number are obtained for various physical parameters.

INTRODUCTION

Viscous fluid motion generated by stagnation point flow occurs in many practical applications such as plastic sheet extrusion, biological process, cooling of metallic plates, thermal oil recovery, etc. Heimenz [1] was the first to elaborate the two-dimensional stagnation point flow. Homann [2] continued this work by considering an axisymmetric three-dimensional flow. Wang [3] studied both two-dimensional and axisymmetric stagnation point flows toward a shrinking sheet in a viscous flow. Mahapatra and Gupta [4] analyzed the heat transfer behavior in a stagnation point flow over a stretching sheet. Stagnation point flow generated by Newtonian heating was reported by Salleh et al. [5]. Different cases of a stagnation point flow over a stretching sheet were studied by Ishak et al. [6], Nazar et al. [7], Bhatti et al. [8] and Zheng et al. [9].

*E-mail: giulio.lorenzini@unipr.it

Heat transfer under convective boundary conditions has appreciable impact on the final product of the manufacturing industries. This study plays a crucial role in the applications like heat exchangers, conjugate heat transfer around fins, etc. Aziz [10] reported the repercussion of convective boundary condition on heat transfer. Makinde and Aziz [11] discussed the internal heat generation effect on a mixed convection flow past a convectively heated vertical plate. Fang et al. [12] illustrated MHD boundary layer flow over a permeable shrinking sheet by taking a velocity slip condition at the surface. Bhattacharya et al. [13] studied the impact of partial slip on stagnation point flow.

Nanofluid is a new type of fluid proposed by Choi [14] at the time of investigations on coolants techniques and cooling processes. These fluids are fascinating a great deal of interest due to their tremendous potential with respect to enhanced heat transfer. Buongiorno [15] developed a new model for nanofluid flow by considering the effects of Brownian motion and thermophoresis. By using this model, Khan and Pop [16] studied the boundary layer flow of a nanofluid over a stretching sheet. Mustafa et al. [17], Ibrahim et al. [18], Bachok et al. [19], and others have analyzed the stagnation point flow of nanofluids. Yacob et al. [20] and Makinde and Aziz [21] have also reported problems on a nanofluid flow over a stretching sheet by taking the convective boundary condition at the surface.

The Casson fluid model [22] is a prominent model for many fluids such as blood, chocolate, honey, etc. Casson fluid behaves as solid when the shear stress is less than the yield stress and it starts to deform when the shear stress becomes greater than the yield stress. Mehta et al. [23] investigated the repercussion of Casson fluid under yield stress through a homogeneous porous medium bounded by a circular tube. Sandeep et al. [24] reported heat and mass transfer behavior of MHD Casson fluid over an exponential permeable stretching surface. Detailed study on Casson nanofluid under various aspects could be found in [25–27].

In this paper, an attempt has been made to study the MHD stagnation point flow of Casson nanofluid over a nonlinear stretching sheet in the presence of velocity ratio, magnetic field, suction, thermal radiation, viscous dissipation, heat generation/absorption, chemical reaction, Brownian motion, thermophoresis, slip and convective boundary conditions. The flow, heat and mass transfer equations are solved using HAM.

MATHEMATICAL FORMULATION

Consider a steady two-dimensional dissipative MHD stagnation point flow of an incompressible Casson nanofluid over a nonlinear stretching sheet, which coincides with the plane $y = 0$. The flow being confined in the region $y \geq 0$. It is assumed that $u = U_w = ax^n$ is the stretching velocity of the sheet and $U_\infty = bx^n$ is the free stream velocity where $a > 0$, $b > 0$ are constants and $n \geq 0$ is the nonlinear stretching parameter. The slip velocity at the surface is taken as $U_{slip} = \left(\mu_B + \frac{p_y}{\sqrt{2\,\pi_c}}\right)\frac{\partial u}{\partial y}$. The temperature of the sheet is regulated by a convective heating process, which is symbolized by a temperature T_f and a heat transfer coefficient h_f. It is assumed that C_w is the nanoparticle concentration and as $y \to \infty$, the ambient values of temperature and nanoparticle concentration are T_∞ and C_∞. A magnetic field $B(x) = B_0 x^{\frac{n-1}{2}}$ is applied perpendicular to the sheet with constant B_0. The rheological equation of state for an isotropic and incompressible flow of Casson fluid is [36]

$$\tau_{ij} = \begin{cases} 2\left(\mu_B + \dfrac{p_y}{\sqrt{2\pi}}\right) e_{ij}, & \pi > \pi_c, \\ 2\left(\mu_B + \dfrac{p_y}{\sqrt{2\pi_c}}\right) e_{ij}, & \pi_c > \pi, \end{cases}$$

where μ_B is the plastic dynamic viscosity of the non-Newtonian fluid, p_y is the yield stress of the fluid, π is the product of the component of deformation rate with itself, $\pi = e_{ij}e_{ij}$, e_{ij} is the $(i,j)^{\text{th}}$ component of the deformation rate and π_c is the critical value of this product based on the non-Newtonian model.

Under these assumptions, the equations governing the flow can be written as:

$$\frac{\partial u}{\partial x} + \frac{\partial v}{\partial y} = 0, \tag{1}$$

$$u\frac{\partial u}{\partial x}+v\frac{\partial u}{\partial y}=\nu\left(1+\frac{1}{\beta}\right)\frac{\partial^2 u}{\partial y^2}+U_\infty\frac{\partial U_\infty}{\partial x}+\frac{\sigma B^2(x)}{\rho_f}\left(U_\infty-u\right), \tag{2}$$

$$u\frac{\partial T}{\partial x}+v\frac{\partial T}{\partial y}=\alpha\frac{\partial^2 T}{\partial y^2}+\frac{(\rho c)_p}{(\rho c)_f}\left[D_B\frac{\partial C}{\partial y}\frac{\partial T}{\partial y}+\frac{D_T}{T_\infty}\left(\frac{\partial T}{\partial y}\right)^2\right]+\frac{\nu}{C_p}\left(1+\frac{1}{\beta}\right)\left(\frac{\partial u}{\partial y}\right)^2$$

$$-\frac{1}{(\rho c)_f}\frac{\partial q_r}{\partial y}+\frac{1}{(\rho c)_f}\frac{Q_0}{(T-T_\infty)}, \tag{3}$$

$$u\frac{\partial C}{\partial x}+v\frac{\partial C}{\partial y}=D_B\frac{\partial^2 C}{\partial y^2}+\frac{D_T}{T_\infty}\frac{\partial^2 T}{\partial y^2}-k_0\left(C-C_\infty\right) \tag{4}$$

subject to the boundary conditions:

$$u=U_w+U_{slip}=ax^n+\left(\mu_B+\frac{p_y}{\sqrt{2\pi_c}}\right)\frac{\partial u}{\partial y},\ \ v=v_w,\ \ -k\frac{\partial T}{\partial y}=h_f(T_f-T),\ \ C=C_w\ \text{ at }\ y=0,$$

$$u\to U_\infty=bx^n,\quad v\to 0,\quad T\to T_\infty,\quad C\to C_\infty\quad\text{as}\quad y\to\infty. \tag{5}$$

Now, we introduce the following similarity transformations to convert the partial differential equations to ordinary differential equations:

$$\left.\begin{aligned}&u=ax^n f'(\xi),\ \xi=y\sqrt{\frac{a(n+1)}{2\nu}}x^{\left(\frac{n-1}{2}\right)},\ v=-\sqrt{\frac{a\nu(n+1)}{2}}x^{\left(\frac{n-1}{2}\right)}\left(f(\xi)+\frac{n-1}{n+1}\xi f'(\xi)\right),\\&\psi=\sqrt{\frac{2a\nu}{(n+1)}}x^{\left(\frac{n+1}{2}\right)}f(\xi),\ \ \theta(\xi)=\frac{T-T_\infty}{T_f-T_\infty},\quad \phi(\xi)=\frac{C-C_\infty}{C_w-C_\infty},\end{aligned}\right\} \tag{6}$$

where ξ is the similarity variable, ψ is the stream function.

The stream function ψ is formalized in the standard way as:

$$u=\frac{\partial\psi}{\partial y},\quad v=-\frac{\partial\psi}{\partial x}.$$

Here we assume $v_w=-\sqrt{\frac{a\nu(n+1)}{2}}x^{\left(\frac{n-1}{2}\right)}S$, where S is the suction parameter.

Substituting Eq. (6) in Eqs. (2) to (5), we obtain

$$\left(1+\frac{1}{\beta}\right)f'''+ff''-\frac{2n}{n+1}\left(f'^2-A^2\right)+M\left(A-f'\right)=0, \tag{7}$$

$$\left(1+\frac{4}{3}R\right)\theta''+\Pr f\theta'+\Pr Nb\theta'\phi'+\Pr Nt\theta'^2+\left(1+\frac{1}{\beta}\right)\Pr Ecf''^2+\Pr Q\theta=0, \tag{8}$$

$$\phi''+Lef\phi'+\frac{Nt}{Nb}\theta''-Le\gamma\phi=0. \tag{9}$$

The boundary conditions are

$$\left.\begin{aligned}&f(0)=S,\quad f'(0)=1+\delta\left(1+\tfrac{1}{\beta}\right)f''(0),\quad \theta'(0)=-Bi\left(1-\theta(0)\right),\quad \phi(0)=1,\\&f'(\infty)\to A,\quad \theta(\infty)\to 0,\quad \phi(\infty)\to 0,\end{aligned}\right\} \tag{10}$$

where the prime denotes differentiation with respect to ξ.

Nondimensional skin friction coefficient C_f, local Nusselt number Nu_x and local Sherwood number Sh_x are

$$C_f = \frac{\tau_w}{\rho U_w^2}, \quad \text{where} \quad \tau_w = \mu_B \left(1 + \frac{1}{\beta}\right) \left(\frac{\partial u}{\partial y}\right)_{y=0}, \quad Nu_x = \frac{x q_w}{k\left(T_f - T_\infty\right)}, \quad \text{and}$$

$$Sh_x = \frac{x q_m}{D_B\left(C_w - C_\infty\right)},$$

where τ_w is the wall shear stress, q_w and q_m are the heat and mass fluxes at the surface, which are defined as:

$$q_w = \left(-\left(k + \frac{16\sigma^* T_\infty^3}{3k^*}\right)\left(\frac{\partial T}{\partial y}\right)\right)_{y=0}, \quad q_m = -D_B \left(\frac{\partial C}{\partial y}\right)_{y=0}.$$

Substituting q_w and q_m in the preceding equations, we get

$$Re_x^{1/2} C_f \sqrt{\frac{2}{n+1}} = \left(1 + \frac{1}{\beta}\right) f''(0), \quad Re_x^{-1/2} Nu_x \sqrt{\frac{2}{n+1}} = -\left(1 + \frac{4}{3}R\right)\theta'(0), \quad \text{and}$$

$$Re_x^{-1/2} Sh_x \sqrt{\frac{2}{n+1}} = -\phi'(0),$$

where $Re_x = \frac{U_w x}{\nu}$ is the local Reynolds number.

HOMOTOPY ANALYSIS METHOD

The equations of flow, temperature and concentration have been solved using HAM. This method has been successfully utilized by many researchers to solve various problems (Liao [28], Sajid and Hayat [29], Mabood et al. [30], Wang et al. [31], Moghimi et al. [32]). To apply this method, the pertinent initial guesses $f_0(\xi)$, $\theta_0(\xi)$, and $\phi_0(\xi)$ and linear operators $L_1(f)$, $L_2(\theta)$, and $L_3(\phi)$ for f, θ, and ϕ are chosen as:

$$f_0(\xi) = S + A\xi + \left(\frac{1 - A}{1 + \delta\left(1 + \frac{1}{\beta}\right)}\right)\left(1 - e^{-\xi}\right),$$

$$\theta_0(\xi) = \left(\frac{Bie^{-\xi}}{1 + Bi}\right), \tag{11}$$

$$\phi_0(\xi) = e^{-\xi}.$$

$$\begin{aligned} L_1(f) &= f''' - f', \\ L_2(\theta) &= \theta'' - \theta, \\ L_3(\phi) &= \phi'' - \phi. \end{aligned} \tag{12}$$

The higher deformation equations corresponding to Eqs. (7) to (9) subject to the boundary conditions (10) can be formulated using (11) and (12) (for details see Liao [33], Abbasbandy [34], Samir [35]) and the appropriate values for the nonzero parameters $\hbar_1$, $\hbar_2$, and $\hbar_3$ have been obtained by plotting the $\hbar$-curves in Fig. 1. Our computations point out that the series converge in the whole region of ξ when $\hbar_1 = \hbar_2 = \hbar_3 = -0.7$. Table 1 exhibits the convergence of the adopted method.

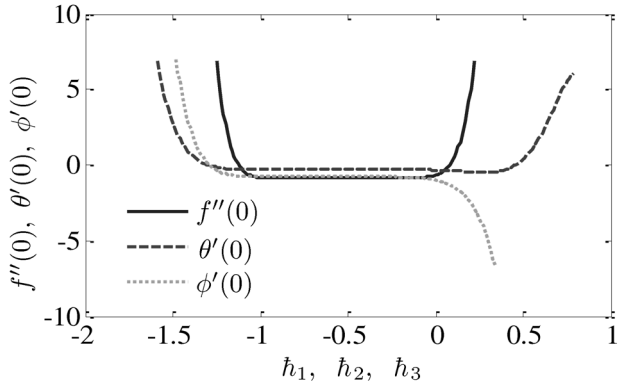

Fig. 1. $\hbar$-curves of $f''(0)$, $\theta'(0)$, and $\phi'(0)$ for 15th-order approximation.

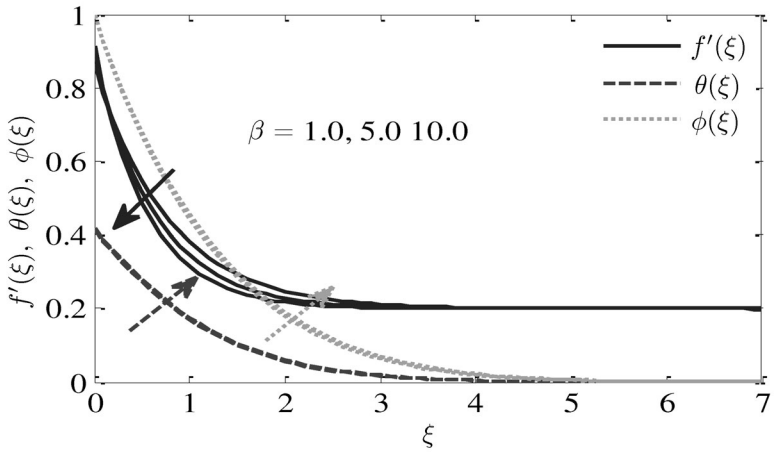

Fig. 2. Effect of β on $f'(\xi)$, $\theta(\xi)$, and $\phi(\xi)$.

Table 1. Convergence of HAM solution for different orders of approximations when $\beta = 1.0$, $n = 2.0$, $S = 1.0$, $A = 0.2$, $M = 0.5$, $\delta = R = Nb = Nt = Ec = Q = 0.1$, $Bi = 0.5$, $Pr = 0.7$, $Le = 0.6$, and $\gamma = 0.2$

Order	$-f''(0)$	$-\theta'(0)$	$-\phi'(0)$
5	0.84995	0.29366	0.78036
10	0.84898	0.29376	0.77286
15	0.84870	0.29377	0.77271
20	0.84871	0.29377	0.77275
25	0.84871	0.29377	0.77275
30	0.84871	0.29377	0.77275
35	0.84871	0.29377	0.77275

RESULTS AND DISCUSSION

This section highlights the influence of arising parameters such as Casson fluid parameter (β), nonlinear parameter (n), magnetic parameter (M), velocity ratio parameter (A), slip parameter (δ), suction parameter (S), thermal radiation (R), Prandtl number (Pr), Brownian motion parameter (Nb), thermophoresis parameter (Nt), viscous dissipation (Ec), heat generation/absorption parameter (Q),

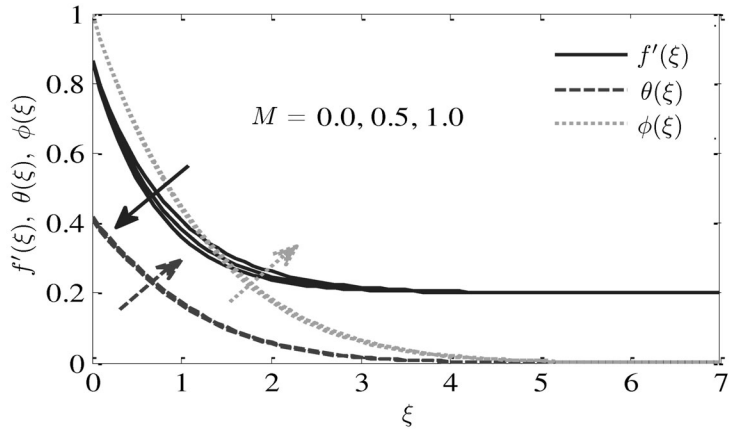

Fig. 3. Effect of M on $f'(\xi)$, $\theta(\xi)$, and $\phi(\xi)$.

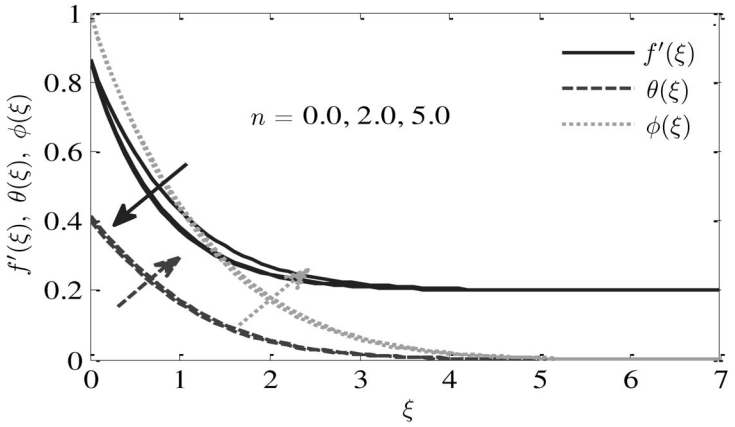

Fig. 4. Effect of n on $f'(\xi)$, $\theta(\xi)$, and $\phi(\xi)$.

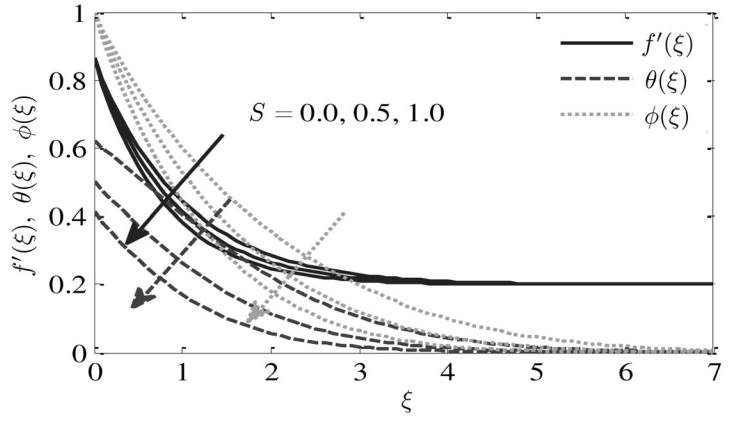

Fig. 5. Effect of S on $f'(\xi)$, $\theta(\xi)$, and $\phi(\xi)$.

Biot number (Bi), Lewis number (Le), and chemical reaction parameter (γ) on velocity, temperature and concentration. Numerical solutions are carried out through HAM. For numerical results we considered

$$\beta = 1.0, \quad n = 2.0, \quad S = 1.0, \quad A = 0.2, \quad M = 0.5, \quad \delta = R = Nb = Nt = Ec = Q = 0.1,$$

$$B_i = 0.5, \quad Pr = 0.7, \quad Le = 0.6, \quad \gamma = 0.2.$$

These values are conserved as common unless specifically pointed out in the appropriate graphs and tables.

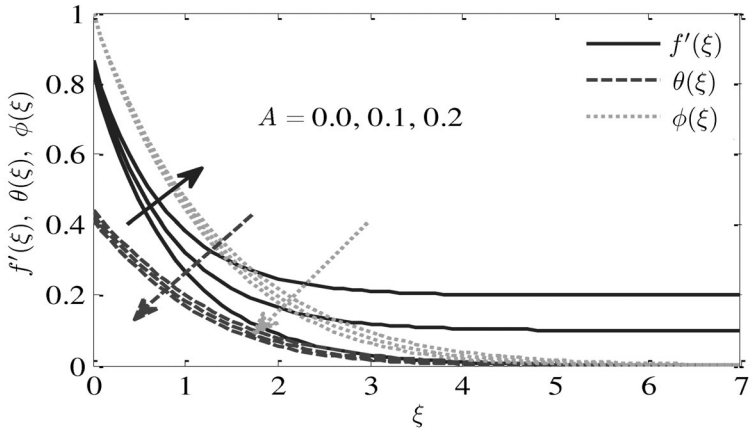

Fig. 6. Effect of A on $f'(\xi)$, $\theta(\xi)$, and $\phi(\xi)$.

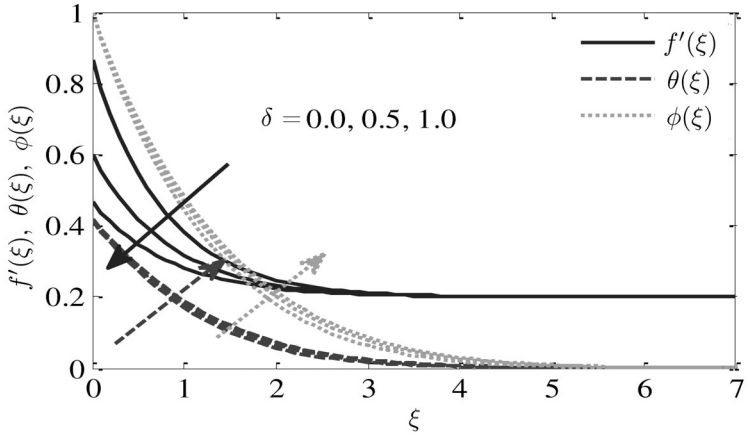

Fig. 7. Effect of δ on $f'(\xi)$, $\theta(\xi)$, and $\phi(\xi)$.

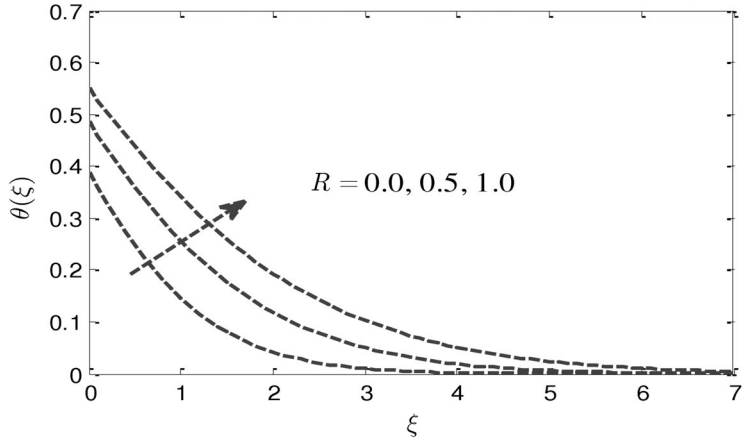

Fig. 8. Effect of R on $\theta(\xi)$.

Figure 2 shows the variation of the Casson fluid parameter β versus velocity, temperature and concentration profiles. As β increases, the plastic dynamic viscosity, which opposes the fluid motion, increases, hence the velocity decreases. Further, thermal resistance on the hot fluid side decreases with β as a result the temperature accelerates. As β increases, Casson fluid behaves like a Newtonian fluid. Thus, the concentration elevates with β.

Figure 3 describes the possession of the magnetic parameter M versus velocity, temperature and

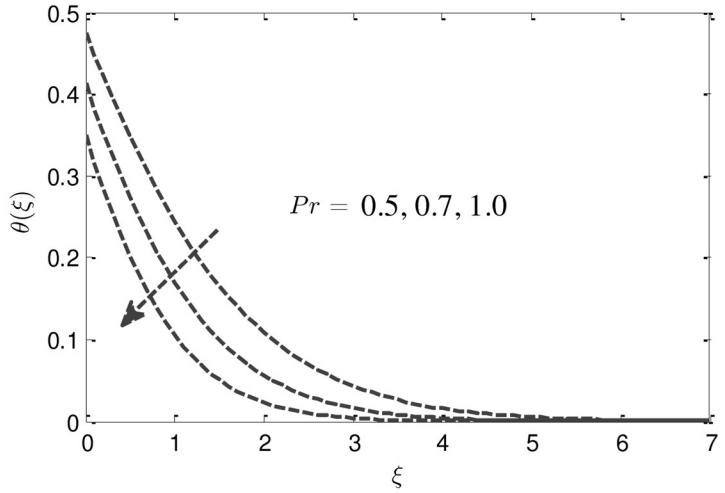

Fig. 9. Effect of Pr on $\theta(\xi)$.

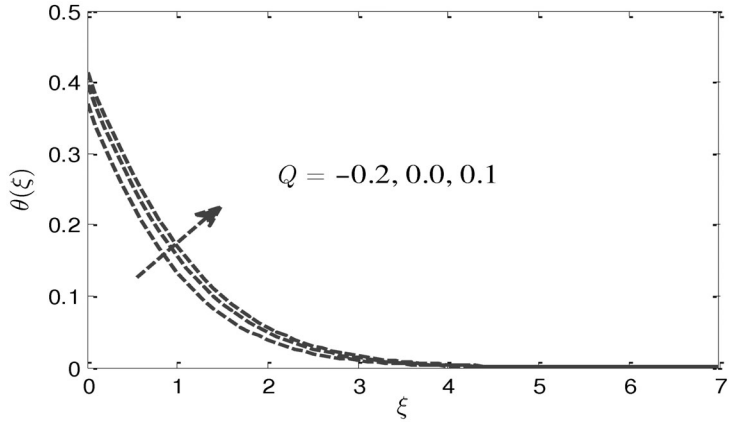

Fig. 10. Effect of Q on $\theta(\xi)$.

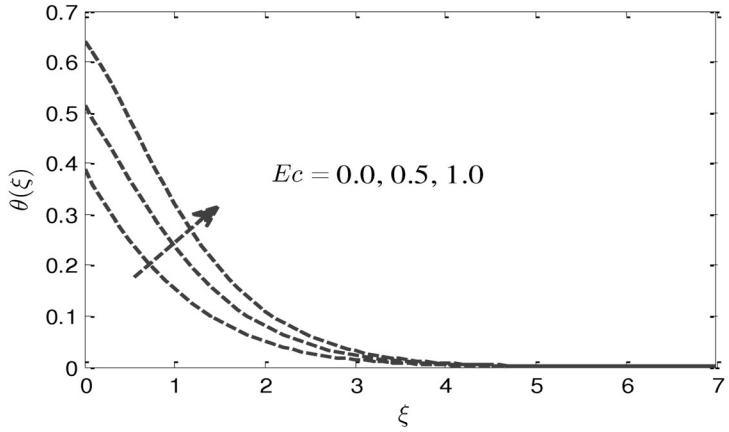

Fig. 11. Effect of Ec on $\theta(\xi)$.

concentration. Velocity decreases with the magnetic parameter M and opposite phenomena is noted in the case of temperature and concentration. This is due to the Lorentz force created by the magnetic field. Velocity, temperature and concentration profiles for different values of the nonlinear stretching parameter n are shown in Fig. 4. It is noticed that the velocity decreases and the temperature and concentration accelerate with the increase of n. Figure 5 illustrates the influence of suction parameter S on velocity,

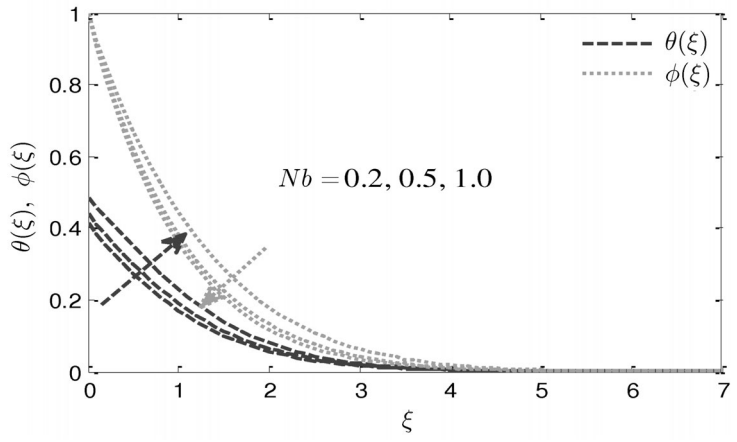

Fig. 12. Effect of Nb on $\theta(\xi)$ and $\phi(\xi)$.

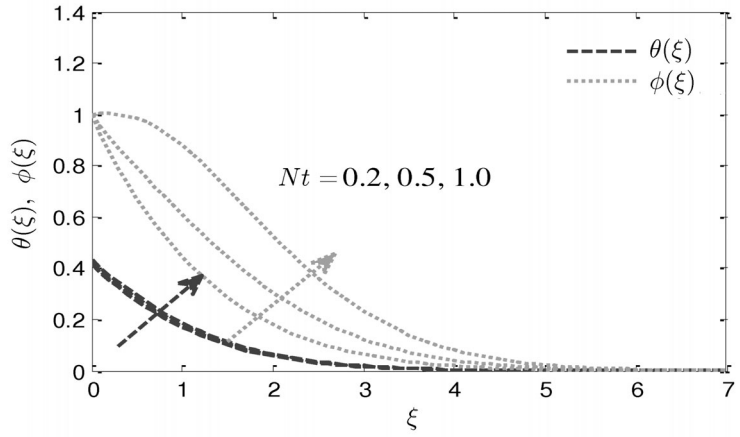

Fig. 13. Effect of Nt on $\theta(\xi)$ and $\phi(\xi)$.

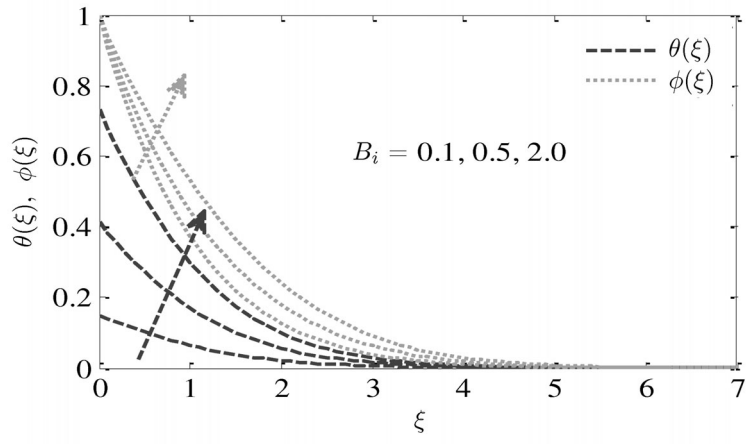

Fig. 14. Effect of B_i on $\theta(\xi)$ and $\phi(\xi)$.

temperature and concentration profiles. The velocity, temperature, and concentration decelerate with the increase of S.

Figure 6 depicts the effect of velocity ratio parameter A on velocity, temperature and concentration. Velocity increases with A and an opposite phenomena is observed for temperature and concentration. An increase in the velocity slip parameter δ causes deceleration in nanofluid velocity and enhancement in both nanofluid temperature and nanoparticle volume fraction. This result is depicted in Fig. 7. The

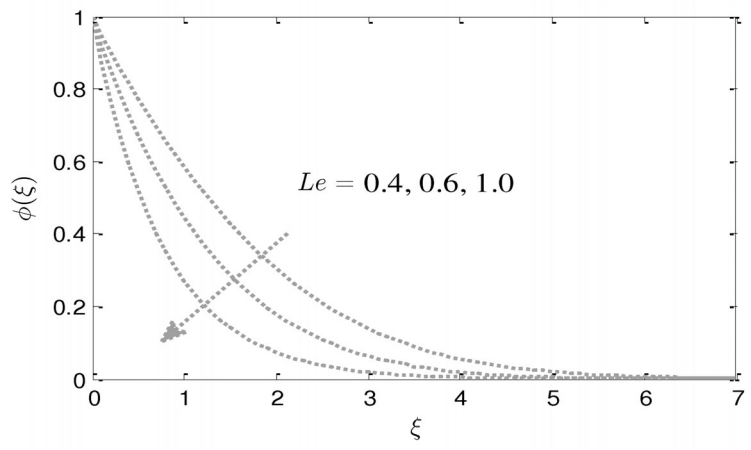

Fig. 15. Effect of Le on $\phi(\xi)$.

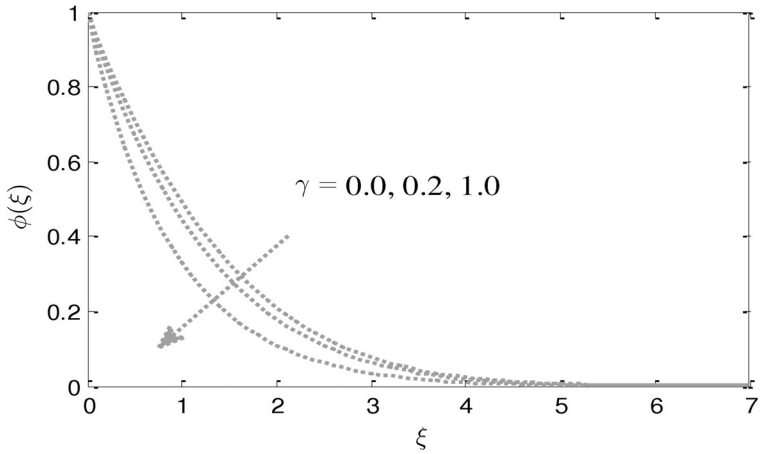

Fig. 16. Effect of γ on $\phi(\xi)$.

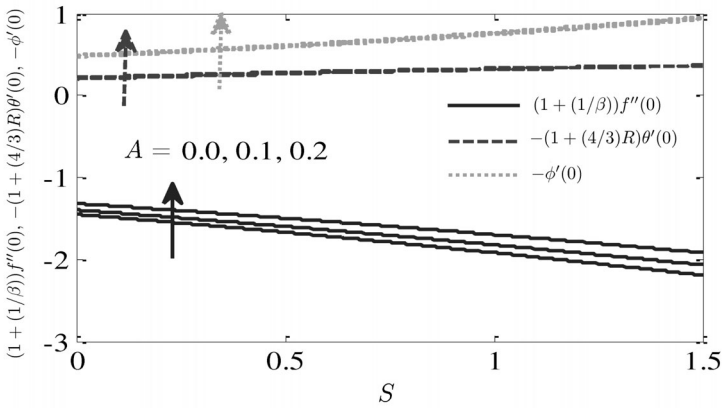

Fig. 17. Effect of A and S on skin friction coefficient, Nusselt number, and Sherwood number.

effect of radiation parameter R on temperature is displayed in Fig. 8. It is noticed that the temperature rises with the increase of R.

An increase in Prandtl number Pr causes an increase in fluid viscosity, which causes reduction in temperature. It is shown in Fig. 9, Fig. 10 shows the effect of heat source/sink parameter on temperature. The figure declares that the temperature declines for negative values of Q (heat sink) due to heat absorption in the thermal boundary layer. In a similar manner heat generation exists in the thermal boundary layer for positive values of Q (heat source) and, hence, temperature increases.

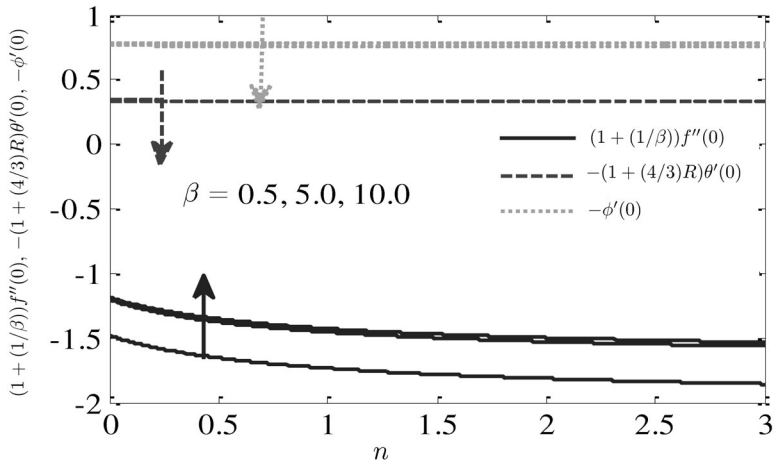

Fig. 18. Effect of n and β on skin friction coefficient, Nusselt number, and Sherwood number.

Table 2. Comparison of skin friction coefficient for different values of β and A when $M = 0$, $\delta = 0.0$, $S = 0.0$, and $n = 1.0$

β	A	Mondal et al. [36]	HAM
1	0.0	−1.41421	−1.41421
5	0.0	−1.09544	−1.09545
1000	0.01	−0.99782	−0.99801
1000	0.1	−0.96937	−0.96937
1000	0.2	−0.91811	−0.91811

Table 3. Comparison of $-f''(0)$ for different values of δ when $M = 0$, $A = 0.0$, $\beta = 1000$, $S = 0.0$, and $n = 1.0$

δ	Ibrahim and Makinde [37]	Mondal et al. [36]	HAM
0.0	1.0000	1.000000	1.00000
0.1	0.8721	0.872083	0.87208
0.2	0.7764	0.776377	0.77638
0.5	0.5912	0.591195	0.59121
1.0	–	0.430160	0.43017
2.0	0.2840	0.283979	0.28397
3.0	–	0.214054	0.21406
5.0	0.1448	0.144714	0.14484
10.0	0.0812	0.080932	0.08125

The influence of Eckert number Ec on temperature is presented in Fig. 11. As Ec increases, the wall temperature also increases due to heat addition by frictional heating. The effect of Brownian motion parameter Nb on temperature and concentration fields is illustrated in Fig. 12. It can be seen that the temperature is increasing and the concentration is decelerating with Nb.

An increase in thermophoresis parameter Nt generates movement in the nanoparticles from the higher temperature region to the lower temperature region in the boundary layer region. Thus, increase

Table 4. Comparison of $-\theta'(0)$ and $-\phi'(0)$ when $M = A = \delta = S = R = Ec = Q = \gamma = 0.0$, $Nb = 0.5$, $Bi = 10000$, $Pr = Le = 2.0$, and $\beta \to \infty$

n	Nt	Rana and Bhargava [38]		Mabood and Khan [39]		HAM	
		$-\theta'(0)$	$-\phi'(0)$	$-\theta'(0)$	$-\phi'(0)$	$-\theta'(0)$	$-\phi'(0)$
0.2	0.3	0.4533	0.8395	0.4520	0.8402	0.45197	0.84011
	0.5	0.3999	0.8048	0.3987	0.8059	0.39905	0.80571
3.0	0.3	0.4282	0.7785	0.4271	0.7791	0.42725	0.77919
	0.5	0.3786	0.8323	0.3775	0.7390	0.37772	0.73878
10	0.3	0.4277	0.7654	0.4216	0.7660	0.42180	0.76598
	0.5	0.3739	0.7238	0.3728	0.7248	0.37309	0.72436

Table 5. Numerical values of skin friction coefficient $-\left(1+\frac{1}{\beta}\right) f''(0)$, Nusselt number $-\left(1+\frac{4}{3}R\right)\theta'(0)$, and Sherwood number $-\phi'(0)$ for different values of δ, R, Nb, Nt, Ec, Q, Bi, and γ

δ	R	Nb	Nt	Ec	Q	Bi	γ	$-\left(1+\frac{1}{\beta}\right) f''(0)$	$-\left(1+\frac{4}{3}R\right)\theta'(0)$	$-\phi'(0)$
0.1	0.1	0.2	0.2	0.1	0.1	0.5	0.2	−1.69743	0.33294	0.77274
0.5								−0.95332	0.33197	0.72178
1.0								−0.61221	0.32883	0.69758
	0.5							–	0.42884	0.81317
	0.7							–	0.46962	0.82831
		0.5						–	0.31795	0.90492
		1.0						–	0.29130	0.94929
			0.3					–	0.33174	0.67008
			0.5					–	0.32929	0.46868
				0.5				–	0.27542	0.83879
				1.0				–	0.20317	0.92169
					−0.2			–	0.35715	0.74643
					0.0			–	0.34220	0.76274
						0.1		–	0.09665	0.92602
						2.0		–	0.60994	0.59416
							0.0	–	0.33348	0.65631
							0.5	–	0.33233	0.91960

in Nt implies an increase in both the temperature and nanoparticle volume fraction as shown in Fig. 13. The advancement of temperature and concentration with the Biot number Bi is illustrated in Fig. 14. This is due to the fact that convective heating, as well as temperature gradient, increases with Bi.

The influences of the Lewis number Le and the chemical reaction parameter γ on the concentration profiles are illustrated in Figs. 15 and 16, respectively. It can be observed that the increase in Le reduces the concentration boundary layer. Similar effect is observed with the increase of γ. From Figs. 17 and 18

it is clear that the skin friction coefficient increases with A, β and decreases with S, n, whereas Nusselt number and Sherwood number are increasing with A, S and decreasing with β, n.

Tables 2, 3, and 4 exhibit an excellent correlation between the present and the previous results under limiting conditions.

The influence of various parameters such as δ, R, Nb, Nt, Ec, Q, B_i, and γ on the skin friction coefficient, Nusselt number and Sherwood number is shown in Table 5. From the table, it is seen that the skin friction coefficient enhances with δ. Nusselt number and Sherwood number enhance with R, and a reverse trend is observed with δ and Nt. Nusselt number declines and Sherwood number rises with Nb, Ec, Q, and γ.

CONCLUSIONS

Some important observations of this study can be summarized as follows:

- Momentum boundary layer becomes thinner as β, M, n, S, and δ increase and thicker as A increases.
- Temperature acts as an increasing function of β, M, n, δ, R, Ec, Q, Nb, Nt, and Bi and decreasing function of S, A, and Pr.
- Nanoparticle volume fraction enhances with β, M, n, δ, Nt, and Bi and declines with S, A, Nb, Le, and γ.

NOTATIONS

u, v—velocity components in x and y directions
k—thermal conductivity
$\alpha = \dfrac{k}{(\rho c)_f}$—thermal diffusivity
σ—electrical conductivity
B_0—constant
ν—kinematic viscosity
β—Casson fluid parameter
ρ_f—density of the base fluid
D_B—Brownian diffusion coefficient
D_T—thermophoresis diffusion coefficient
Q_0—volumetric heat generation/absorption
C_p—specific heat at constant pressure
T—fluid temperature
C—fluid concentration
k_0—chemical reaction coefficient
v_w—velocity of suction
ψ—stream function
T_w—wall temperature
C_w—nanoparticle concentration
T_∞—ambient value of temperature
C_∞—ambient value of the nanoparticle fraction
$(\rho c)_f$—heat capacity of the fluid
$(\rho c)_p$—effective heat capacity of a nanoparticle
n—nonlinear stretching parameter
a, b—positive constants
$U_w = ax^n$—stretching velocity
$U_\infty = bx^n$—free stream velocity

$U_{slip} = \left(\mu_B + \frac{p_y}{\sqrt{2\pi_c}}\right)\frac{\partial u}{\partial y}$—slip velocity

$B(x)$—magnetic field

$A = \frac{b}{a}$—velocity ratio parameter

$\delta = \mu_B\sqrt{\frac{a(n+1)}{2\nu}}x^{\frac{n-1}{2}}$—slip parameter

$Bi = \frac{h_f}{k}\sqrt{\left(\frac{2\nu}{a(n+1)}\right)}\frac{1}{x^{\frac{n-1}{2}}}$—Biot number

$M = \frac{2\sigma B_0^2}{a\rho_f(n+1)}$—magnetic parameter

$\mathrm{Pr} = \frac{\nu}{\alpha}$—Prandtl number

$R = \frac{4\sigma^* T_\infty^3}{k^* k}$—radiation parameter

$Nb = \frac{(\rho c)_p D_B (C_w - C_\infty)}{\nu(\rho c)_f}$—Brownian motion parameter

$Nt = \frac{(\rho c)_p D_T (T_f - T_\infty)}{\nu(\rho c)_f T_\infty}$—thermophoresis parameter

$Ec = \frac{U_w^2}{C_p(T_f - T_\infty)}$—Eckert number

$Q = \frac{2xQ_0}{(\rho c)_f (n+1) U_w}$—heat generation/absorption coefficient

$Le = \frac{\nu}{D_B}$—Lewis number

$\gamma = \frac{2\nu x k_0}{(n+1)U_w}$—chemical reaction parameter

$S = -\frac{v_w}{\sqrt{\frac{a\nu(n+1)}{2}}x^{(\frac{n-1}{2})}}$—suction parameter

Subscripts

w—condition at the surface

∞—condition at the free stream

REFERENCES

1. Hiemenz, K., Die Grenzschicht an einem in den gleichformingen Flussigkeitsstrom eingetauchten graden Kreiszylinder, *Dingler's Polytech. J.*, 1911, no. 326, pp. 321–324,
2. Homann, F., Der Einfluss grosser Zähigkeit bei der Strömung um den Zylinder und um die Kugel, *Zeits. Ang. Math. Mech.*, 1936, no. 16, pp. 153–164,
3. Wang, C.Y., Stagnation Flow towards a Shrinking Sheet, *Int. J. Non-Lin. Mech.*, 2008, vol. 43, pp. 377–382,
4. Mahapatra, T.R. and Gupta, A.S., Heat Transfer in Stagnation-Point Flow towards a Stretching Sheet, *Heat Mass Transfer*, 2002, vol. 38, pp. 517–521.
5. Mohamed, M.K.A., Salleh, M.Z., Nazar, R., and Ishak, A., Stagnation Point Flow over a Stretching Sheet with Newtonian Heating, *Sains Malaysiana*, 2012, vol. 41, pp. 1467–1473,
6. Ishak, A., Jafar, K., Nazar, R., and Pop, I., MHD Stagnation Point Flow towards a Stretching Sheet, *Phys. A: Statist. Mech. Appl.*, 2009, vol. 388, pp. 3377–3383.
7. Ali, F.M., Nazar, R., Arifin, N.M., and Pop, I., MHD Stagnation-Point Flow and Heat Transfer towards Stretching Sheet with Induced Magnetic Field, *Appl. Math. Mech.*, 2011, vol. 32, pp. 409–418.

8. Bhatti, M.M., Abbas, T., and Rashidi, M.M., A New Numerical Simulation of MHD Stagnation-Point Flow over a Permeable Stretching/Shrinking Sheet in Porous Media with Heat Transfer, *Iranian J. Sci. Technol., Trans. A: Sci.*, 2016, vol. 1, pp. 1–7.
9. Zhu, J., Zheng, L.C., and Zhang, Z.G., Effects of Slip Condition on MHD Stagnation-Point Flow over a Power-Law Stretching Sheet, *Appl. Math. Mech.*, 2010, vol. 31, pp. 439–448.
10. Aziz, A., A Similarity Solution for Laminar Thermal Boundary Layer over a Flat Plate with a Convective Surface Boundary Condition, *Comm. Nonlin. Sci. Numer. Simul.*, 2009, vol. 14, pp. 1064–1068.
11. Makinde, O.D. and Aziz, A., Mixed Convection from a Convectively Heated Vertical Plate to a Fluid with Internal Heat Generation, *J. Heat Transfer*, 2011, vol. 133, pp. 1–6.
12. Fang, T., Zhang, J., and Yao, S., Slip Magnetohydrodynamic Viscous Flow over a Permeable Shrinking Sheet, *Chinese Phys. Lett.*, 2010, vol. 27, pp. 1–4.
13. Bhattacharyya, K., Mukhopadhyay, S., and Layek, G.C., Slip Effects on Boundary Layer Stagnation-Point Flow and Heat Transfer towards a Shrinking Sheet, *Int. J. Heat Mass Transfer*, 2011, vol. 54, pp. 308–313.
14. Choi, S.U.S., Enhancing Thermal Conductivity of Fluids with Nanoparticles, *Proc. 1995 ASME Int. Mechanical Engineering Congress and Exposition, San Francisco, CA: ASME, FED*, 1995, vol. 231, pp. 99–105,
15. Buongiorno, J., Convective Transport in Nanofluids, *J. Heat Transfer*, 2006, vol. 128, pp. 240–250.
16. Khan, W.A. and Pop, I., Boundary-Layer Flow of a Nanofluid past a Stretching Sheet, *Int. J. Heat Mass Transfer*, 2010, vol. 53, pp. 2477–2483.
17. Mustafa, M., Hayat, T., Pop, I., Asghar, S., and Obaidat, S., Stagnation-Point Flow of a Nanofluid towards a Stretching Sheet, *Int. J. Heat Mass Transfer*, 2011, vol. 54, pp. 5588–5594.
18. Ibrahim, W., Shankar, B., and Nandeppanavar, M.M., MHD Stagnation Point Flow and Heat Transfer Due to Nanofluid towards a Stretching Sheet, *Int. J. Heat Mass Transfer*, 2013, vol. 56, pp. 1–9.
19. Bachok, N., Ishak, A., and Pop, I., Stagnation-Point Flow over a Stretching/Shrinking Sheet in a Nanofluid, *Nanosc. Res. Lett.*, 2013, vol. 6, pp. 1–10.
20. Yacob, N.A., Ishak, A., Pop, I., and Vajavelu, K., Boundary Layer Flow past a Stretching/Shrinking Surface beneath an External Uniform Shear Flow with a Convective Surface Boundary Condition in a Nanofluid, *Nanosc. Res. Lett.*, 2011, vol. 6, pp. 1–7.
21. Makinde, O.D. and Aziz, A., Boundary Layer Flow of a Nanofluid past a Stretching Sheet with a Convective Boundary Conditions, *Int. J. Therm. Sci.*, 2011, vol. 50, pp. 1326–1332.
22. Casson, N., A Flow Equation for Pigment Oil Suspensions of the Printing Ink Type, in *Rheology of Disperse Systems*, Mill, C.C., Ed., New York: Pergamon, 1959, pp. 84–102.
23. Dash, R.K., Mehta, K.N., and Jayaraman, G., Effect of Yield Stress on the Flow of a Casson Fluid in a Homogeneous Porous Medium Bounded by Circular Tube, *Appl. Sci. Res.*, 1996, vol. 57, pp. 133–149.
24. Raju, C.S.K., Sandeep, N., Sugunamma, V., Jayachandra Babu, M., and Ramana Reddy, J.V., Heat and Mass Transfer in Magnetohydrodynamic Casson Fluid over an Exponentially Permeable Stretching Surface, *Eng. Sci. Technol. Int. J.*, 2016, vol. 19, pp. 45–52.
25. Mustafa, M. and Khan, J.A., Model for Flow of Casson Nanofluid past a Non-Linearly Stretching Sheet Considering Magnetic Effects, *AIP Adv.*, 2015, vol. 5, pp. 1–11.
26. Pal, D., Roy, N., and Vajravelu, K., Effects of Thermal Radiation and Ohmic Dissipation on MHD Casson Nanofluid Flow over a Vertical Non-Linear Stretching Surface Using Scaling Group Transformation, *Int. J. Mech. Sci.*, 2016, vol. 114, pp. 257–267.
27. Mabood, F., Shateyi, S., and Khan, W.A., Effects of Thermal Radiation on Casson Flow Heat and Mass Transfer around a Circular Cylinder in Porous Medium, *European Phys. J.-Plus*, vol. 130, no. 188, 2015.
28. Liao, S.J., *Beyond Perturbation: Introduction to Homotopy Analysis Method*, Boca Raton: Chapman and Hall, CRC Press, 2011.
29. Sajid, M. and Hayat, T., Influence of Thermal Radiation on the Boundary Layer Flow Due to an Exponentially Stretching Sheet, *Int. Commun. Heat Mass Transfer*, 2008, vol. 35, pp. 347–356.
30. Mabood, F., Khan, W.A., and Ismail, A.I.M., Multiple Slips Effects on MHD Casson Fluid Flow in Porous Media with Radiation and Chemical Reaction, *Canadian J. Phys.*, 2015, vol. 94, no. 1, pp. 26–34.
31. Gao, L., Wang, J., Zhing, Z., and Du, J., An Analysis of Surface Acoustic Wave Propagation in Functionally Graded Plates with Homotopy Analysis Method, *Acta Mech.*, 2009, vol. 208, pp. 249–258.
32. Moghimi, S.M., Domairry, G., Soleimani, S., Ghasemi, E., and Bararnia, H., Application of Homotopy Analysis Method to Solve Jeffery–Hamel Flows in Non-Parallel Walls, *Adv. Eng. Soft.*, 2011, vol. 42, pp. 108–113.
33. Liao, S.J., *Homotopy Analysis Method in Nonlinear Differential Equations*, Heidelberg: Springer & Higher Education Press, 2012.
34. Abbasbandy, S., The Application of Homotopy Analysis Method to Nonlinear Equations Arising in Heat Transfer, *Phys. Lett. A*, 2006, vol. 360, pp. 109–113.

35. Samir Kumar, N., Analytical Solution of MHD Stagnation-Point Flow and Heat Transfer of Casson Fluid over a Stretching Sheet with Partial Slip, *ISRN Thermodyn.*, 2013, vol. 2013, pp. 1–9.
36. Oyelakin, I.S., Mondal, S., and Sibanda, P., Unsteady Casson Nanofluid Flow over a Stretching Sheet with Thermal Radiation, Convective and Slip Boundary Conditions, *Alexandria Eng. J.*, 2016, vol. 55, pp. 1025–1035.
37. Ibrahim, W. and Makinde, O.D., Magnetohydrodynamic Stagnation Point Flow and Heat Transfer of Casson Nanofluid past a Stretching Sheet with Slip and Convective Boundary Conditions, *J. Aerospace Eng.*, 2016, vol. 29, pp. 1–11.
38. Rana, P. and Bhargava, R., Flow and Heat Transfer of a Nanofluid over a Nonlinearly Stretching Sheet: A Numerical Study, *Comm. Nonlin. Sci. Numer. Simul.*, 2012, vol. 17, pp. 212–226.
39. Mabood, F., Khan, W.A., and Ismail, A.I.M., MHD Boundary Layer Flow and Heat Transfer of Nanofluids over a Nonlinear Stretching Sheet: A Numerical Study, *J. Magn. Magn. Mater.*, 2015, vol. 374, pp. 569–576.